Enteroendocrine K Cells Exert Complementary Effects to Control Bone Quality and Mass in Mice

Benoît Gobron, Béatrice Bouvard, Sagar Vyavahare, Liv Vv V V Blom, Kristian K Pedersen, Johanne A Windeløv, Geke A Boer, Norio Harada, Sheng Zhang, Satoko Shimazu-kuwahara, et al.

▶ **To cite this version:**

Benoît Gobron, Béatrice Bouvard, Sagar Vyavahare, Liv Vv V V Blom, Kristian K Pedersen, et al.. Enteroendocrine K Cells Exert Complementary Effects to Control Bone Quality and Mass in Mice. Journal of Bone and Mineral Research, 2020, 35 (7), pp.1363-1374. 10.1002/jbmr.4004 . hal-02946043

HAL Id: hal-02946043

https://univ-angers.hal.science/hal-02946043

Submitted on 22 Sep 2020

HAL is a multi-disciplinary open access archive for the deposit and dissemination of scientific research documents, whether they are published or not. The documents may come from teaching and research institutions in France or abroad, or from public or private research centers.

L'archive ouverte pluridisciplinaire **HAL**, est destinée au dépôt et à la diffusion de documents scientifiques de niveau recherche, publiés ou non, émanant des établissements d'enseignement et de recherche français ou étrangers, des laboratoires publics ou privés.

Enteroendocrine K-cells exert complementary effects to control bone quality and mass in mice

B. Gobron[1,2], B. Bouvard[1,2], S. Vyavahare[3], L.V.V. Blom[4], K.K. Pedersen[4], J.A. Windeløv[4,5], G.A. Boer[4,5], N. Harada[6], S. Zhang[7], S. Shimazu-Kuwahara[6], B. Wice[7], N. Inagaki[6], , E. Legrand[1,2], P.R. Flatt[3], D. Chappard[1,8,9], B. Hartmann[4,5], J.J. Holst[4,5], M.M. Rosenkilde[4], N. Irwin[3], G. Mabilleau[1,8,9]

[1] Groupe études remodelage osseux et biomatériaux, GEROM, SFR 42-08, Université d'Angers, Institut de Biologie en Santé, CHU d'Angers, 49933 Angers cedex, France.

[2] Service de Rhumatologie, CHU d'Angers, 49933 Angers cedex, France

[3] School of Biomedical Sciences, University of Ulster, BT52 1SA Coleraine, Northern Ireland, United Kingdom

[4] Department of Biomedical Sciences, University of Copenhagen, 2200 Copenhagen, Denmark

[5] Novo Nordisk Foundation Center for Basic Metabolic Research, University of Copenhagen, Copenhagen, Denmark

[6] Department of Diabetes, Endocrinology and Nutrition, Kyoto University Graduate School of Medicine, Kyoto 606-8507, Japan

[7] Department of Internal Medicine, Division of Endocrinology, Metabolism and Lipid Research Washington University School of Medicine, 63110 Saint Louis, MO United States of America

[8] Service commun d'imageries et d'analyses microscopiques, SCIAM, SFR 42-08, Université d'Angers, Institut de Biologie en Santé, CHU d'Angers, 49933 Angers cedex, France

[9] Bone pathology Unit, CHU d'Angers, 49933 Angers cedex, France

Please send all correspondence to:

Guillaume Mabilleau, PhD
GEROM-LHEA UPRES EA 4658
Institut de Biologie en Santé
Université d'Angers
4 rue larrey
49933 Angers Cedex 09
France

☎ : +33(0) 244 688 450
Fax : +33(0) 244 688 451
✉ : guillaume.mabilleau@univ-angers.fr

DISCLOSURE

Dr B. Hartmann is a minority shareholder of Bainan Biotech. Professor J. J. Holst is a minority shareholder and board member of Antag Therapeutics and Bainan Biotech and has been a consultant for, served on scientific advisory panels of and as speaker honoraria for Novo Nordisk and MSD/Merck. Professor M.M. Rosenkilde is a minority shareholder of and consultant for Antag Therapeutics, Bainan Biotech and Synklino. None of the other authors have a conflict of interest to report.

ABSTRACT

The involvement of a gut-bone axis in controlling bone physiology has been long suspected, although the exact mechanisms are unclear. We explored whether glucose-dependent insulinotropic polypeptide (GIP)-producing enteroendocrine K-cells were involved in this process. The bone phenotype of transgenic mouse models lacking GIP secretion (GIP-GFP-KI) or enteroendocrine K-cells (GIP-DT) was investigated. Mice deficient in GIP secretion exhibited lower bone strength, trabecular bone mass, trabecula number and cortical thickness, notably due to higher bone resorption. Alterations of microstructure, modifications of bone compositional parameters, represented by lower collagen cross-linking were also apparent. None of these alterations were observed in GIP-DT mice lacking enteroendocrine K-cells, suggesting that other K-cell secretory product acts to counteract GIP action. To assess this, stable analogues of the known K-cell peptide hormones, xenin and GIP, were administered to mature NIH Swiss male mice. Both were capable of modulating bone strength mostly by altering bone microstructure, bone gene expression and bone compositional parameters. However, the two molecules exhibited opposite actions on bone physiology, with evidence that xenin effects are mediated indirectly, possibly via neural networks. Our data highlight a

previously unknown interaction between GIP and xenin, which both moderate gut-bone connectivity.

Keywords: GIP, Xenin, Bone remodeling, Enteroendocrine system

1. INTRODUCTION

A hormonal regulation of bone metabolism by the gastrointestinal tract has previously been proposed, based on the rapid reduction in circulating bone resorption markers after feeding [1]. However, the mechanism linking these two organs has not been clearly established. The bone turnover response to oral glucose administration is much greater than to intravenous glucose administration, supporting a role for the gastrointestinal tract in modulating bone remodeling [2]. Attempts to identify key molecules have highlighted the possible involvement of two types of enteroendocrine cells (EEC), namely K- and L-cells. K-cells, located mostly in the duodenal epithelium [3], are responsible for secretion of glucose-dependent insulinotropic polypeptide (GIP) [4]. A role for GIP in modulating circulating markers of bone resorption in humans is supported by recent investigations [5]. GIP receptor (GIPr) knockout animals have provided further information on the effects of GIP on bone metabolism [6-8]. Although all these investigations have highlighted a link between the GIPr and bone remodeling, conflicting data obscure a clear understanding of the GIP/GIPr pathway on skeletal physiology.

The original classification of EEC was based on their major secretory products and is still used today. However, we know now that EECs often secrete more than a single peptide product. The L-cells secrete the proglucagon products GLP-1, GLP-2, and oxyntomodulin and often also PYY, whereas GIP-secreting K-cells also may produce xenin, cholecystokinin, somatostatin and secretin [9,10]. However, the possible actions of these additional K-cell products in bone metabolism has never been studied previously.

The main objective of this study was to decipher the role of K-cell secretory products in bone physiology. In order to ascertain whether K-cells are involved in the control of bone physiology, we used a murine model of K-cell ablation, i.e. mice expression of diphtheria toxin under the control of the GIP promoter. We also administered synthetic GIP, xenin, cholecystokinin, secretin or a somatostatin receptor agonist to healthy mice, to better

understand how these peptides regulate bone remodeling. Finally, we also used a validated murine model of GIP secretion invalidation to decipher further its role in the regulation of bone physiology. We found that GIP and xenin were the only bone-active molecules and that they exerted different, but complementary, actions on bone physiology. These K-cell secretory product findings shed important new light on the role of the gut-bone axis.

2. MATERIAL AND METHODS

2.1. Reagents

[D-Ala^2]GIP$_{1-42}$, xenin-25(Lys^{13}PAL) and secretin analogues were purchased from GeneCust Europe with a purity >95% (Dudelange, Luxembourg). (pGlu-Gln)CCK-8 was purchased from Thermofisher scientific (Waltham, Massachusetts, United States). The somatostatin analogue, RC160, was purchased from Tocris Biosciences (Lille, France). Purity and sequences of peptides were verified by HPLC and matrix-assisted laser desorption ionization-time of flight (MALDI-TOF) mass spectrometry, respectively. Activity of all peptides was verified prior to administration to animals by quantifying cAMP response in receptor-expressing CHO-K1 cells. M-CSF (catalog number 216-MC) and soluble human RANKL (catalog number 390-TN) were purchased from Bio-techne (Lille, France). All other chemicals were obtained from Sigma-Aldrich (Lyon, France), unless otherwise stated.

2.2 Animals

All procedures were approved and conducted in accordance with either the Institutional Animal Care and Use committees of the University of Angers (Angers, France) or with Danish Animal Experiments Inspectorate (License # 2018-15-0201-01397). Male GIP-GFP-KI (C57BL/6J background, n=8)) and their age and sex-matched wild-type littermates (n=8) were obtained from Kyoto University (Kyoto, Japan). GIP-DT (C57BL/6J background, n=9) mice and their

age and sex-matched wild-type littermates (n=6) were obtained from the Washington University school of medicine (Saint-Louis, MO, USA). All transgenic and corresponding wild-type littermates were used at 16 weeks of age. Design and generation of transgenic animals have been described in detail elsewhere [11,12]. Thirty-four 21-week-old NIH Swiss male mice (strain NIH/OlaHsd) were obtained from Envigo (Wooley Road, Huntington, Alconbury PE28 4HS, UK). Male Swiss mice were randomly allocated into six groups that received once daily, by subcutaneous administration, saline (n=6), [D-Ala²]GIP$_{1-42}$ (25 nmoles/kg) (n=6), xenin-25(Lys^{13}PAL) (25 nmoles/kg) (n= 5), (pGlu-Gln)CCK-8 (25 nmoles/kg) (n=5), secretin (25 nmoles/kg) (n=6) or RC160 (30 microg/kg) (n=6) for 6 weeks. These peptides, doses and regimen of administration were selected based on our extensive experience of gut peptide analogues or from the literature [13-16]. Twelve 16-week-old NIH Swiss male mice (strain NIH/OlaHsd) were obtained from Envigo and randomly allocated into two groups that received once daily, by subcutaneous administration, saline (n=6) or a coadministration of [D-Ala²]GIP$_{1-42}$ (25 nmoles/kg) and xenin-25(Lys^{13}PAL) (25 nmoles/kg) (n= 6) for 4 weeks. Sixteen-week old C57BL/6 male mice were obtained from the Department of Experimental Medicine at the University of Copenhagen and randomly allocated into two groups that received once daily saline (n=6) or xenin-25(Lys^{13}PAL) (25 nmoles/kg, n=6) for 4 weeks.

Animals were maintained in a 12 h: 12 h light: dark cycle and had free access to water and standard rodent diet (Diet A04, Safe, Augy, France). Mice received calcein (10 mg/kg bw; ip) 10 and 3 days before being culled. Animals were overnight fasted (16h) before being sacrificed by intracardiac blood collection (~250µl) into EDTA-treated microtubes (Sarstedt) and cervical dislocation. Blood samples were then spun at 13,000g for 15 min, aliquoted and stored at -80°C. After necropsy, tibias and femurs were collected and cleaned of soft tissue. Left tibias were fixed in 4% formaldehyde for 24 hours and then stored in 70% ethanol for microCT and histomorphometry. Left femurs were wrapped in saline-soaked gauze and stored at -20°C until

three-point bending tests. Right tibias and femurs were immersed in RNAlater (Invitrogen, Illkirch, France) and snap-frozen in liquid nitrogen before being stored at -80°C until use. Identity of the mice and their treatment were not revealed until the end of all measurements.

2.3. Biochemical analyses

Plasma levels of C-terminal telopeptide of collagen type I (CTx-I – RatLaps, Immunodiagnostic Systems Ltd, Boldon, UK), N-terminal propeptide of type I collagen (P1NP - Rat/mouse P1NP, Immunodiagnostic Systems Ltd), Insulin-like growth factor-1 (IGF-1 – IGF-1 Quantikine, Biotechne, Lille, France), parathyroid hormone (PTH, Eurobio, Les Ulis, France), total glucagon-like peptide-1 (GLP-1, Merck Millipore, Molsheim, France) and total GIP (Merck Millipore) were measured according to the manufacturers' recommendation.

2.4. X-ray microcomputed tomography

MicroCT analyses were performed using the left tibia with a Skyscan 1272 microtomograph (Bruker-Skyscan, Kontich, Belgium) operated at 70 kV, 100 μA, 340 ms integration time. The isotropic pixel size was fixed at 3.8 μm, the rotation step at 0.25° and exposure was performed with a 0.5-mm aluminum filter. Each 3D reconstruction image dataset was binarized using global thresholding. The trabecular volume of interest was located 0.5 mm below the growth plate and extended 2 mm down. The cortical volume of interest was located 3 mm below the growth plate and extended at a height of 1 mm. All histomorphometrical parameters were measured according to guidelines and nomenclature proposed by the American Society for Bone and Mineral Research [(17)].

2.5. Bone histomorphometry

After microCT scans, left tibias were embedded, undecalcified in pMMA at 4°C to preserve enzyme activities. For each animal, four non serial longitudinal sections (~50 µm apart) were left unstained for the measurement of calcein-based parameters and four additional sections were stained for the osteoclastic tartrate resistant acid phosphatase (TRAcP), as previously described [18]. Standard bone histomorphometrical nomenclatures, symbol and units were used as described in the guidelines of the American Society for Bone and Mineral Research [19]. The identity of the sections was not revealed until the end of all measurements.

2.6. Assessment of bone strength

Whole-bone strength was assessed by 3-point bending on left femurs as described previously [8,20]. Three-point bending strength was measured with a constant span length of 10 mm. Bones were tested in the antero-posterior axis with the posterior surface facing upward, centered on the support and the pressing force was applied vertically to the midshaft of the bone. Each bone was tested with a loading speed of 2 $mm.min^{-1}$ until failure with a 500 N load cell on an Instron 5942 device (Instron, Elancourt, France) and the load-displacement curve was recorded at a 100 Hz rate by the Bluehill 3 software (Instron). Ultimate load, ultimate displacement, stiffness and work to fracture were calculated as indicated in [21]. The yield load was calculated with the 0.2% offset method. Post-yield displacement was also computerized.

Strength at the tissue level was assessed by nanoindentation of the tibia on pMMA blocks used for bone histomorphometry. Prior to nanoindentation, blocks were rehydrated for 24 h in saline at 4°C. Eight indents were positioned in cortical bone with a NHT-TTX system (CSM, Peseux, Switzerland) equipped with a Berkovich diamond probe as previously described [8]. Indentation depth was fixed at 900 nm with a loading/ unloading rate of 40 mN/min. At maximum load, a holding period of 15 seconds was applied to avoid creeping of the bone material. Maximum

load, indentation modulus, hardness and dissipated energy were determined according to Oliver and Pharr [22].

2.7. Quantitative backscattered electron imaging (qBEI)

Quantitative backscattered electron imaging was done on the same blocks and regions as nanoindentation as previously reported [23]. The cortical bone area was imaged at a 200× nominal magnification, corresponding to a pixel size of 0.5 μm per pixel. The region of interest corresponded to 2-mm centered in the midshaft femur (6 mm below the growth plate). The gray levels distribution of each image was analyzed with a lab-made routine using ImageJ. Three variables were obtained from the bone mineral density distribution: Ca_{peak} is the most frequently observed calcium concentration, Ca_{mean} is the average calcium concentration and Ca_{width} is the width of the histogram at half maximum of the peak.

2.8. Fourier Transform Infrared Microscopy (FTIRM)

FTIRM experiments were performed on 4 μm thick sections of the pMMA blocks used for nanoindentation. After sandwiching the sections between BaF2 optical windows, spectral analysis was performed using a Bruker Vertex 70 spectrometer (Bruker optics, Ettlingen, Germany) interfaced with a Bruker Hyperion 3000 infrared microscope equipped with a standard single element Mercury Cadmium Telluride (MCT) detector. Infrared spectra were recorded at a resolution of 4 cm^{-1}, with an average of 32 scans in transmission mode in the same location as qBEI and nanoindentation as previously reported [8]. For FTIRM analysis, 12 spectra were acquired between double calcein labels (animal study only) and analyzed with a lab-made routine in Matlab R2016b. Briefly, Mie scattering contribution was removed using the RMieS-EMSC algorithm (kind gift from Prof Gardner, University of Manchester). Then, spectra were baseline fitted and second derivative spectroscopy was applied as reported

previously [24]. The evaluated parameters were the mineral-to-matrix ratio (900-1200 cm^{-1}/Amide I) [25]; mineral maturity (1030/1020 cm^{-1}) [26]; carbonate-to-phosphate ratio (820-890cm^{-1} /900-1200 cm^{-1}) [27]; acid phosphate content (1127 cm^{-1}/1096 cm^{-1}) [28] and collagen maturity (1660/1690 cm^{-1}) [25]. Bone sections were then demineralized with EDTA during 7 days as reported previously [29] and reanalyzed at the same locations to determine the collagen glycation (1032 cm^{-1}/Amide I) [24].

2.9. Isolation and osteoclast generation from human peripheral blood mononuclear cells (PBMCs)

Peripheral Blood Mononuclear Cells (PBMCs) were isolated from 3 buffy coats obtained at the Etablissement Francais du Sang (Angers, France) as previously described [30]. To assess the extent of osteoclast formation and activation, isolated human PBMCs were cultured either in 24-well plates or collagen-coated 24 well plates at a concentration of 2 x 10^6 PBMCs/ml in MEM containing 1g/L glucose, 100 UI/ml penicillin, 100 µg/ml streptomycin and 10% FCS (osteoclast medium) [31]. After 2 h incubation, cultures were vigorously rinsed in medium to remove non-adherent cells, and then maintained in 1 ml osteoclast medium with 25 ng/ml recombinant human M-CSF, 30 ng/ml recombinant human sRANKL (added at day 7) and various concentrations of GIP or xenin.

2.10. Osteoblast cultures

MC3T3-E1 cells were purchased from American Type Culture Collection (ATCC, Teddington, UK) and grown as recommended in propagation medium containing αMEM supplemented with 5% FBS, 5% bovine calf serum, 100 UI/mL penicillin, and 100 µg/mL streptomycin in a humidified atmosphere enriched with 5% CO_2 at 37 °C. For differentiation studies, cells were detached with trypsin-EDTA, plated at a density of 1.5×10^4 cells/cm^2 and grown to confluence

in propagation medium. At confluence, the propagation medium was replaced by the differentiation medium containing αMEM supplemented with 5% FBS, 5% bovine calf serum, 100 U/mL penicillin, 100 µg/mL streptomycin, 50 µg/mL ascorbic acid and various concentrations of GIP or xenin. Osteoblast cultures were then fixed in absolute ethanol, scrapped off the culture dish and transferred onto BaF2 windows where they were air-dried. For FTIRM analysis, 20 spectra were acquired and analyzed as above. Collagen maturity was determined.

2.11. Gene expression

Tibias were rapidly cleaned of soft tissues and fibula before the distal end was cut off. Tibias were then centrifuged for 20s at 16,000g at room temperature in nested microcentrifuge tubes as reported previously in detail [32]. Total RNA was extracted by crushing bones in Nucleozol (Macherey-Nagel, Hoerdt, France) and purifying total RNA with Nucleospin RNA set nucleozol column (Macherey-Nagel) according to the manufacturer's recommendations. Total RNA was reversed transcribed using iScript cDNA synthesis kit (Bio-Rad) and amplified by real-time PCR using SYBR Green PCR master mix (Bio-Rad). The expression level of each sample was normalized against *gapdh* mRNA expression.

2.12. Statistical analysis

Statistical analyses were performed with GraphPad Prism 6.01 (GraphPad Software, La Jolla, CA, USA). Two-tailed unpaired t-tests were used to compare differences between WT and GIP-DT mice, WT and GIP-GFP-KI animals, C57BL/6 mice treated with saline or xenin, and Swiss mice administered with saline or both GIP and xenin analogues. Analyses of variance with Dunnett post-hoc test were employed to compare differences between saline and K-cell product

analogues groups in Swiss mice, and in *in vitro* experiments. Differences at $p<0.05$ were considered significant.

3. RESULTS

3.1. Ablation of K-cells results in normal bone phenotype despite absence of GIP secretion.

First, we looked at the bone phenotype of mice deficient in K-cells (GIP-DT). These mice have been originally developed to study whether mice lacking K-cells were protected from obesity induced by a high fat diet. As previously reported, the diphtheria toxin A chain gene was inserted in exon 2 of the *Gip* gene under control by the GIP promoter [12]. These animals exhibit normal levels of other incretin hormones, GLP-1 and GLP-2 [12]. These animals did not present any modifications of body weight or growth as compared with WT littermates (Supplementary Table 1). However, despite absence of GIP secretion, GIP-DT mice did not exhibit any alterations of bone strength at the whole-bone level (Figure 1A and Supplementary Table 1). This lack of effect was corroborated by absence of significant changes in both trabecular and cortical microarchitectures, and in osteoblast activity and osteoclast counts (Figure 1B-D and Supplementary Table 1). No differences in either the bone matrix strength or the bone matrix composition were observed between GIP-DT mice and WT littermates (Figure 1E-F and Supplementary Table 1). These results suggested that genetic ablation of enteroendocrine K-cell does not alter skeletal physiology.

3.2. GIP is a potent and positive modulator of bone mass and quality

Based on the previous investigation of GIPr KO animals, where alterations of bone mass and quality were evidenced [6,8], the lack of bone alterations in GIP-DT mice was surprising and unexpected. We therefore decided to explore further the role of the GIP/GIPr pathway in skeletal physiology by using a model of genetic GIP ablation. The GIP-GFP-KI mouse has a GFP cassette inserted in exon 3 of the GIP gene under the control of the GIP promoter. As a

result, these mice are defective in the expression and secretion of GIP but not of other gut hormones including GLP-1 and GLP-2 [33]. KI animals did not present with any modifications of body weight or growth as compared with WT littermates (Supplementary Table 2). Whole bone strength was not significantly altered in these animals (Figure 2A and Supplementary Table 2), although a trend for lower stiffness (p=0.070) was noted. Trabecular and cortical microarchitectures were significantly altered following genetic ablation of GIP production as represented by lower BV/TV (-22%, p=0.0006), Tb.N (-21%, p<0.001) and Ct.Th (-13%, p=0.009), and higher Tb.Sp (8%, p=0.014) (Figure 2B-C and Supplementary Table 2). Osteoblast activity was not significantly affected although the bone formation rate exhibited a trend towards higher values, but importantly, osteoclast counts, and surfaces were significantly higher in KI mice (32%, p=0.015; 42%, p=0.015, respectively) (Figure 2D and Supplementary Table 2). Bone matrix mechanical properties were also altered in KI animals as evidenced by lower values for indentation force (-16%, p=0.038) and hardness (-18%, p=0.053) (Figure 2E and Supplementary Table 2). Investigation of bone composition revealed a significant reduction in collagen crosslinking at bone formation sites as shown by a 23% reduction in collagen maturity (p=0.003). On the other hand, bone mineral quantity, distribution and properties were not significantly different between the two groups of animals (Figure 2F and Supplementary Table 2). These observations suggest that lack of GIP leads to an accelerated bone remodeling and loss of bone mass and quality, but also supports previous findings in GIPr KO animals [6-8].

GIP and xenin, but no other K-cell products, are important for bone physiology

In light with the above skeletal observations following genetic ablation of GIP expression in GIP-GFP-KI mice, the skeletal phenotype of GIP-DT mice was striking. We hypothesized that an explanation could reside in the skeletal actions of another K-cell product. To investigate this

in more detail, we looked at whether receptors for other K-cell products, namely xenin, cholecystokinin, secretin and somatostatin, were expressed in bone tissues. Only GIPr was found in bone (Figure 3A). However, the action of another K-cell product could be indirect and in order to investigate this, we administered stable analogues of K-cell products in normal Swiss NIH mice.

As compared with saline controls, whole bone strength was only significantly modified in GIP- and xenin-injected mice as demonstrated by significant higher maximum bending load (+18%, p=0.021) and lower stiffness (-19%, p=0.024), respectively (Figure 3B and Supplementary Table 3). Trabecular but not cortical microarchitectures were significantly altered following GIP or xenin administration with opposite effects being observed with these two molecules (Figure 3C-D and Supplementary Table 3). Indeed, GIP administration resulted in a 26% higher trabecular bone mass and a better organization of the trabecular microarchitecture. Xenin-treated mice presented with a lower trabecular bone mass and a disruption of the trabecular network. Osteoblast activity, determined by histomorphometry or serum markers of bone formation, was augmented in the presence of the GIP analogue and reduced in the presence of the xenin analogue (Figure 3E and Supplementary Table 3). On the other hand, osteoclast counts and activity were reduced by administration of both peptides (Figure 3E and Supplementary Table 3). However, ionized calcium, PTH and IGF-1 levels were not significantly different between saline-, GIP- or xenin-treated mice (Figure 3E). Gene expression in bone confirmed the above observations as GIP administration led to increased expression of osteoblast genes (*Runx2*, +275%; *Atf4*, +224%; *Col1a1* +317%; *Bglap2* +183%) and decreased expression of osteoclast genes (*Nfatc1*, -42%; *Acp5*, -31%; *Ctsk*, -28%; *Mmp9*, -36%). Xenin administration led to decreases in the expression of both osteoclast and osteoblast genes (Figure 3F).

Investigation of bone composition revealed moderate modifications of the mineral phase in the presence of xenin, that resulted in lower (-40%) carbonate substitution (Figure 3G and Supplementary Table3). The organic phase was altered by GIP and xenin with higher (13%) and lower (-38%) collagen crosslinking, respectively. These results are in agreement with the gene expression profile of osteoblast genes implicated in bone matrix maturation (Figure 3H). None of the other K-cell products had any effect on either bone microarchitecture, bone cell activity or bone compositional parameters. Interestingly, xenin analogue administration did not alter GIP or GLP-1 secretion (Figure 3I).

Co-administration of GIP and xenin analogues recapitulates the bone phenotype of GIP-DT mice

We next ascertained whether the effects of xenin was restricted to the Swiss strain or whether we could reproduce it in another strain such as C57BL/6. As compared with saline, administration of xenin analogue to C57BL/6 mice resulted in significant deteriorations of biomechanical responses, microarchitectures and bone tissue composition (Figures 4A-4E).

We also investigated whether co-administration of GIP and xenin analogues in Swiss mice could recapitulate the bone phenotype of GIP-DT mice. As compared with saline-treated animals, co-administration of [D-Ala^2]GIP$_{1-42}$ and xenin-25(Lys^{13}PAL) resulted in no apparent bone phenotype (Figures 4F-I). These observations support dual and opposite actions of two different K-cell-produced hormone in skeletal physiology and could explain the absence of bone phenotype in GIP-DT mice.

GIP but not xenin exerts direct effects on bone cell cultures

In order to determine whether the observed actions of GIP and xenin were exerted directly or indirectly on bone cells, we looked at the effects of adding these peptides to osteoblast and

osteoclast cultures. The expression of the *Gipr* gene was confirmed in RANKL-derived human osteoclasts and in MC3T3-E1 osteoblasts. However, the presence of a functional receptor for any of the other K-cell products was negative in both cell types. The number of newly generated osteoclasts (N.Oc/well) was significantly reduced when GIP was added to the cultures at concentrations of 1 nmol/L and greater (-12%, p=0.036). These findings were confirmed by the decrease in specific osteoclast gene expression such as *Acp5*, *Nfatc1*, *Ctsk* and *Mmp9*. On the other hand, the administration of xenin did not have any effect on the number of osteoclasts or specific osteoclast gene expression.

In osteoblast cultures, GIP administration resulted in significant increases in collagen maturity at a concentration equal to or greater than 100 pmol/L (+108%, p<0.0001) and in specific osteoblast gene expression of *Alpl*, *Col1a1*, *Lox* and *Plod2*. On the other hand, xenin did not affect any of these parameters (Figure 5). These results support a direct action of GIP on bone cells. However, the lack of modifications in any of the above parameters with xenin rule out a direct action on bone cells and suggest that the observed in vivo modifications of skeletal phenotype were due to indirect action on bone.

4. DISCUSSION

A gut-to-bone axis has previously been proposed based on observed changes in the pattern of circulating bone remodelling markers after feeding. Oral glucose exerts a greater decrease in bone resorption than intravenous glucose administration and food fractionation has been shown to increase bone mass [1,2,34]. Among all possible intestinal signalling pathways, enteroendocrine K-cells represent a good candidate for mediating these effects based on the profile of GIP secretion and action that matches the temporal reduction in bone resorption. Previous studies attempting to decipher the role of the GIP/GIPr in modulating bone physiology in rodents have led to contradictory results, with some studies reporting positive and others negative effects on

bone [6-8]. In the present study, we clearly demonstrated that GIP is crucial in order to obtain an optimal bone strength, and that the action of this pathway might be at least partly mediated through direct actions on bone cells. Termination of GIP secretion in mice resulted in clear, negative effects on bone at the molecular level, as represented by lower collagen maturation, but also at the structural level, with bone loss and abnormal trabecular bone microarchitecture. The consequences of these alterations are compromised bone strength and hence a higher fracture risk. These data are supported by recent human studies where a higher prevalence of non-vertebral fractures have been encountered in humans with a single amino acid substitution (rs1800437) in the GIPr that resulted in a decreased receptor activity [35,36].

Consistent with this, transgenic GIP-GFP-KI mice with defective expression and secretion of GIP [11] exhibited clear abnormalities in bone physiology. Similar disturbances have been reported in GIPr KO mice [6-8,37]. However, no such abnormalities were observed in transgenic GIP-DT mice, deficient in GIP due to total ablation of K-cells [12]. It is worth noting that K-cell depletion in GIP-DT mice does not result in any changes in gut hormones expression secreted by other entero-endocrine cells [12].

This discrepancy suggested the possibility that K-cells produce other secretory products that might counter the effects of GIP deficiency. In examining other such peptides, we evidenced that xenin is involved in the control of bone remodelling and quality, exerting an action that is opposed to GIP. Xenin is a 25 amino acid peptide structurally related to neurotensin [38] and previous studies suggest that xenin binds the neurotensin receptor 1 [39,40]. Xenin is mainly secreted by K-cells although recent evidences suggested that a subset of enterochromaffin cells, located in the proximal small intestine, express xenin [10,41]. However, it is worth noting that previously we evidenced that GIP-DT mice had reduced circulating levels of GIP and xenin following oral glucose challenge [42].

Although relatively poorly explored, xenin principal action is believed to be modulation of satiety and gastrointestinal transit, with possible additional regulatory effects on insulin and glucagon secretion [43]. The observed anorexigenic effect of xenin are mediated through the neurotensin receptor 1 [44] and as such it is plausible that xenin acts as a bone catabolic hormone in order to maintain calcium homeostasis. To date, neurotensin receptors have not been found at the surface of bone cells and gene expression analysis in the present study confirmed these findings. The neurotensin receptor 1 null mice exhibit a hyperphagic and overweight phenotype, but possible skeletal alterations in these mice have not yet been studied [45,46].

Furthermore, addition of xenin in osteoblast or osteoclast cultures did not alter the physiology of these cells, suggesting that the observed effects of xenin on bone in vivo results from indirect actions. Xenin has been postulated to exert its effects through neural pathways in the ventromedial hypothalamus [47-49]. A heterogeneous population of neurons is found in the VMH, nevertheless, VMH-residing SF-1 and Htr2c neurons have already been implicated in the control of bone remodeling by lowering bone resorption through enhanced sympathetic nervous system tone or reducing bone formation and increased bone resorption through AP1 blockade [50,51]. The bone phenotype observed in xenin-administered mice in the present study suggests a primarily inhibition of anabolic pathways (35% reduction in circulating P1NP levels) with lower magnitude effects on catabolic pathways (25% reduction in CTx levels). However, further investigations will be required to assess whether or not these effects are related to the VMH.

In addition, Xenin potentiates GIP-mediated insulin secretion partially through a local cholinergic relay [42,52]. Indeed, although, coadministration of GIP and Xenin, in GIP-DT mice, enhances plasma insulin levels by 5.5-fold, the addition of atropine sulfate, a competitive antagonist of muscarinic acetylcholine receptors resulted only in a 1.8-fold decrease in this parameter [42]. This observation suggests the existence of another way of action of Xenin that

potentially could also affect bone remodeling. Expression of muscarinic receptors has been found in osteoblasts and osteoclasts and activation of these surface receptors lead to higher bone formation while there was a lack of effect on osteoclast cultures [53,54]. These actions do not fit with the bone phenotype observed after Xenin administration and it is unlikely that higher cholinergic tone is responsible for the Xenin-mediated bone phenotype observed in the present study. Previously, the action of gut-derived dopamine, on beta cells of the pancreas and on diabetic osteoblasts, has been shown to be part of a negative feedback control of GIP-stimulated insulin secretion and GIP-stimulated LOX expression and bone mass [55,56]. The kinetics of gut-derived dopamine production or secretion coincides with the postprandial rise of GIP plasma levels [56]. As such one could postulate that Xenin might potentialize the secretion of dopamine from the gut. Although, we did not measure dopamine plasma levels in Xenin-treated mice, this scenario seems unlikely with respect to the additive action of Xenin and GIP on insulin secretion [42,52]. Clearly, more research is needed to decipher how this peptide exerts its negative action on bone.

The opposite action of GIP and Xenin on bone metabolism may appear contradictory with their cooperative action on insulin secretion [42,52]. However, it is worth noting that xenin has already been shown to exert biphasic response, as for example a rapid relaxation followed by a slower contraction of the jejunum musculature in guinea pig, by action on distinct neural pathways [39]. A recent growing body of evidences suggest that enteroendocrine cells secrete more than one active hormone product [57]. For example, L-cells secrete PYY as well as neurotensin, GLP-1, GLP-2 and oxyntomodulin derived from differential processing of proglucagon [58,59]. Together these peptides exert several actions including inhibition of feeding, regulation of endocrine pancreatic function and promotion of intestinal growth [60-62]. There is evidence that PYY, GLP-1 and neurotensin are stored in separate secretory vesicles and are released with non-identical

dynamics, suggesting the possibility that the stimuli triggering their secretion or the molecular pathways are different [58,63]. Differences in plasma half-life and clearance of these peptides also result in different temporal hormonal responses following feeding. If the same proves to be true in K-cells for GIP and xenin, and with the biphasic action of xenin observed on the jejunum musculature, then it is possible to envisage a scenario wherein early secretion and elevation of GIP exerts positive action on bone and that subsequent later action of xenin forms part of a natural negative feedback mechanism (Figure 6). Further studies are clearly needed to test this hypothesis and establish the broader physiology of xenin.

Interestingly, none of the other possible K-cell peptide products, namely cholecystokinin, secretin and somatostatin were able to modulate bone physiology at the structural or even the compositional levels. These findings allow us to narrow our focus on relatively few hormones regarding the regulation of bone remodelling by enteroendocrine cells.

A limitation to this study is that we did not investigate whether the same phenotype was encountered in female animals. However, we previously demonstrated that no sexual dimorphism was present in the bone phenotype of GIPr KO mice [7]. Furthermore, previous investigation in metabolic disturbances observed in GIP-DT mice did not evidence either a sexual dimorphism [12,42]. As such it is unlikely that the observed bone phenotype described in the present study is restricted only to male animals.

In conclusion, the present study clearly demonstrated that secretory products of enteroendocrine K-cells play an important role in the modulation of bone physiology. Further studies are required to better understand the involvement of GIP, xenin and other K-cell products in bone turnover and in bone disorders.

5. ACKNOWLEDGEMENTS

The authors are grateful to Nadine Gaborit and Stéphanie Lemière (LUNAM Université, GEROM-LHEA, Institut de Biologie en Santé, Angers, France) for their help with microCT and Prof. Peter Gardner (University of Manchester) for providing the RMieS-EMSC algorithm. The authors also thank the personnel of the animal care facility (LUNAM University-SCAHU) for their help with animal handling and injection. This project was supported by an institutional grant from the University of Angers (to G.M.), Research Challenge and Proof of Principle funding from the University of Ulster (to P.R.F., N.I.).

6. REFERENCES

1. Henriksen DB AP, Bjarnason NH, Vilsbøll T, Hartmann B, Henriksen EE, Byrjalsen I, Krarup T, Holst JJ, Christiansen C. Role of gastrointestinal hormones in postprandial reduction of bone resorption. J Bone Miner Res. 2003;18(12):2180-9.
2. Bjarnason NH, Henriksen EE, Alexandersen P, Christgau S, Henriksen DB, Christiansen C. Mechanism of circadian variation in bone resorption. Bone. 2002;30(1):307-13.
3. Drucker DJ. The biology of incretin hormones. Cell Metab. 2006;3(3):153-65.
4. Baggio LL, Drucker DJ. Biology of incretins: GLP-1 and GIP. Gastroenterology. 2007;132(6):2131-57.
5. Nissen A, Christensen M, Knop FK, Vilsboll T, Holst JJ, Hartmann B. Glucose-dependent insulinotropic polypeptide inhibits bone resorption in humans. J Clin Endocrinol Metab. 2014;99(11):E2325-9.
6. Xie D, Cheng H, Hamrick M, et al. Glucose-dependent insulinotropic polypeptide receptor knockout mice have altered bone turnover. Bone. 2005;37(6):759-69.

7. Gaudin-Audrain C, Irwin N, Mansur S, et al. Glucose-dependent insulinotropic polypeptide receptor deficiency leads to modifications of trabecular bone volume and quality in mice. Bone. 2013;53(1):221-30.

8. Mieczkowska A, Irwin N, Flatt PR, Chappard D, Mabilleau G. Glucose-dependent insulinotropic polypeptide (GIP) receptor deletion leads to reduced bone strength and quality. Bone. 2013;56(2):337-42.

9. Habib AM, Richards P, Cairns LS, et al. Overlap of endocrine hormone expression in the mouse intestine revealed by transcriptional profiling and flow cytometry. Endocrinology. 2012;153(7):3054-65.

10. Anlauf M, Weihe E, Hartschuh W, Hamscher G, Feurle GE. Localization of xenin-immunoreactive cells in the duodenal mucosa of humans and various mammals. J Histochem Cytochem. 2000;48(12):1617-26.

11. Suzuki K, Harada N, Yamane S, et al. Transcriptional regulatory factor X6 (Rfx6) increases gastric inhibitory polypeptide (GIP) expression in enteroendocrine K-cells and is involved in GIP hypersecretion in high fat diet-induced obesity. J Biol Chem. 2013;288(3):1929-38.

12. Althage MC, Ford EL, Wang S, Tso P, Polonsky KS, Wice BM. Targeted ablation of glucose-dependent insulinotropic polypeptide-producing cells in transgenic mice reduces obesity and insulin resistance induced by a high fat diet. J Biol Chem. 2008;283(26):18365-76.

13. Gault VA, Martin CM, Flatt PR, Parthsarathy V, Irwin N. Xenin-25[Lys13PAL]: a novel long-acting acylated analogue of xenin-25 with promising antidiabetic potential. Acta Diabetol. 2015;52(3):461-71.

14. Gault VA, Porter DW, Irwin N, Flatt PR. Comparison of sub-chronic metabolic effects of stable forms of naturally occurring GIP(1-30) and GIP(1-42) in high-fat fed mice. J Endocrinol. 2011;208(3):265-71.

15. Irwin N, Frizelle P, Montgomery IA, Moffett RC, O'Harte FPM, Flatt PR. Beneficial effects of the novel cholecystokinin agonist (pGlu-Gln)-CCK-8 in mouse models of obesity/diabetes. Diabetologia. 2012;55(10):2747-58.

16. Karashima T, Cai RZ, Schally AV. Effects of highly potent octapeptide analogs of somatostatin on growth hormone, insulin and glucagon release. Life Sci. 1987;41(8):1011-9.

17. Bouxsein ML, Boyd SK, Christiansen BA, Guldberg RE, Jepsen KJ, Muller R. Guidelines for assessment of bone microstructure in rodents using micro-computed tomography. J Bone Miner Res. 2010;25(7):1468-86.

18. Chappard D, Alexandre C, Riffat G. Histochemical identification of osteoclasts. Review of current methods and reappraisal of a simple procedure for routine diagnosis on undecalcified human iliac bone biopsies. Basic Appl Histochem. 1983;27(2):75-85.

19. Dempster DW, Compston JE, Drezner MK, et al. Standardized nomenclature, symbols, and units for bone histomorphometry: a 2012 update of the report of the ASBMR Histomorphometry Nomenclature Committee. J Bone Miner Res. 2013;28(1):2-17.

20. Ammann P, Badoud I, Barraud S, Dayer R, Rizzoli R. Strontium ranelate treatment improves trabecular and cortical intrinsic bone tissue quality, a determinant of bone strength. J Bone Miner Res. 2007;22(9):1419-25.

21. Turner CH, Burr DB. Basic biomechanical measurements of bone: a tutorial. Bone. 1993;14(4):595-608.

22. Oliver WC, Pharr GM. An improved technique for determining hardness and elastic modulus using load and displacement sensing indentation experiments. J Mater Res. 1992;7:1564-83.

23. Mabilleau G, Mieczkowska A, Irwin N, et al. Beneficial effects of a N-terminally modified GIP agonist on tissue-level bone material properties. Bone. 2014;63:61-8.

24. Mieczkowska A, Bouvard B, Chappard D, Mabilleau G. Glucose-dependent insulinotropic polypeptide (GIP) directly affects collagen fibril diameter and collagen cross-linking in osteoblast cultures. Bone. 2015;74C:29-36.

25. Paschalis EP, Verdelis K, Doty SB, Boskey AL, Mendelsohn R, Yamauchi M. Spectroscopic characterization of collagen cross-links in bone. J Bone Miner Res. 2001;16(10):1821-8.

26. Paschalis EP, DiCarlo E, Betts F, Sherman P, Mendelsohn R, Boskey AL. FTIR microspectroscopic analysis of human osteonal bone. Calcif Tissue Int. 1996;59(6):480-7.

27. Boskey AL, DiCarlo E, Paschalis E, West P, Mendelsohn R. Comparison of mineral quality and quantity in iliac crest biopsies from high- and low-turnover osteoporosis: an FT-IR microspectroscopic investigation. Osteoporos Int. 2005;16(12):2031-8.

28. Spevak L, Flach CR, Hunter T, Mendelsohn R, Boskey A. Fourier transform infrared spectroscopic imaging parameters describing acid phosphate substitution in biologic hydroxyapatite. Calcif Tissue Int. 2013;92(5):418-28.

29. Mieczkowska A, Mansur SA, Irwin N, Flatt PR, Chappard D, Mabilleau G. Alteration of the bone tissue material properties in type 1 diabetes mellitus: A Fourier transform infrared microspectroscopy study. Bone. 2015;76:31-9.

30. Mabilleau G, Sabokbar A. Interleukin-32 promotes osteoclast differentiation but not osteoclast activation. PLoS One. 2009;4(1):e4173.

31. Mabilleau G, Chappard D, Sabokbar A. Role of the A20-TRAF6 axis in lipopolysaccharide-mediated osteoclastogenesis. J Biol Chem. 2011;286(5):3242-9.

32. Kelly NH, Schimenti JC, Patrick Ross F, van der Meulen MC. A method for isolating high quality RNA from mouse cortical and cancellous bone. Bone. 2014;68:1-5.

33. Nasteska D, Harada N, Suzuki K, et al. Chronic reduction of GIP secretion alleviates obesity and insulin resistance under high-fat diet conditions. Diabetes. 2014;63(7):2332-43.

34. Li F, Muhlbauer RC. Food fractionation is a powerful tool to increase bone mass in growing rats and to decrease bone loss in aged rats: modulation of the effect by dietary phosphate. J Bone Miner Res. 1999;14(8):1457-65.

35. Torekov SS, Harslof T, Rejnmark L, et al. A functional amino acid substitution in the glucose-dependent insulinotropic polypeptide receptor (GIPR) gene is associated with lower bone mineral density and increased fracture risk. J Clin Endocrinol Metab. 2014;99(4):E729-33.

36. Fortin JP, Schroeder JC, Zhu Y, Beinborn M, Kopin AS. Pharmacological characterization of human incretin receptor missense variants. J Pharmacol Exp Ther. 2010;332(1):274-80.

37. Tsukiyama K, Yamada Y, Yamada C, et al. Gastric inhibitory polypeptide as an endogenous factor promoting new bone formation after food ingestion. Mol Endocrinol. 2006;20(7):1644-51.

38. Araki K, Tachibana S, Uchiyama M, Nakajima T, Yasuhara T. Isolation and structure of a new active peptide xenopsin on rat stomach strip and some biogenic amines in the skin of Xenopus laevis. Chem Pharm Bull (Tokyo). 1975;23(12):3132-40.

39. Feurle GE, Klein A, Hamscher G, Metzger JW, Schuurkes JA. Neurokinetic and myokinetic effects of the peptide xenin on the motility of the small and large intestine of guinea pig. J Pharmacol Exp Ther. 1996;278(2):654-61.

40. Feurle GE, Metzger JW, Grudinski A, Hamscher G. Interaction of xenin with the neurotensin receptor of guinea pig enteral smooth muscles. Peptides. 2002;23(3):523-9.

41. Sterl K, Wang S, Oestricker L, et al. Metabolic responses to xenin-25 are altered in humans with Roux-en-Y gastric bypass surgery. Peptides. 2016;82:76-84.

42. Wice BM, Wang S, Crimmins DL, et al. Xenin-25 potentiates glucose-dependent insulinotropic polypeptide action via a novel cholinergic relay mechanism. J Biol Chem. 2010;285(26):19842-53.

43. Craig SL, Gault VA, Irwin N. Emerging therapeutic potential for xenin and related peptides in obesity and diabetes. Diabetes Metab Res Rev. 2018:e3006.

44. Kim ER, Mizuno TM. Role of neurotensin receptor 1 in the regulation of food intake by neuromedins and neuromedin-related peptides. Neurosci Lett. 2010;468(1):64-7.

45. Kim ER, Leckstrom A, Mizuno TM. Impaired anorectic effect of leptin in neurotensin receptor 1-deficient mice. Behavioural brain research. 2008;194(1):66-71.

46. Remaury A, Vita N, Gendreau S, et al. Targeted inactivation of the neurotensin type 1 receptor reveals its role in body temperature control and feeding behavior but not in analgesia. Brain research. 2002;953(1-2):63-72.

47. Cline MA, Nandar W, Rogers JO. Xenin reduces feed intake by activating the ventromedial hypothalamus and influences gastrointestinal transit rate in chicks. Behavioural brain research. 2007;179(1):28-32.

48. Kim ER, Mizuno TM. Xenin delays gastric emptying rate and activates the brainstem in mice. Neurosci Lett. 2010;481(1):59-63.

49. Cooke JH, Patterson M, Patel SR, et al. Peripheral and central administration of xenin and neurotensin suppress food intake in rodents. Obesity (Silver Spring). 2009;17(6):1135-43.

50. Karsenty G, Oury F. The central regulation of bone mass, the first link between bone remodeling and energy metabolism. J Clin Endocrinol Metab. 2010;95(11):4795-801.

51. Idelevich A, Sato K, Nagano K, Rowe G, Gori F, Baron R. Neuronal hypothalamic regulation of body metabolism and bone density is galanin dependent. The Journal of clinical investigation. 2018;128(6):2626-41.

52. Taylor AI, Irwin N, McKillop AM, Patterson S, Flatt PR, Gault VA. Evaluation of the degradation and metabolic effects of the gut peptide xenin on insulin secretion, glycaemic control and satiety. J Endocrinol. 2010;207(1):87-93.

53. Liu PS, Chen YY, Feng CK, Lin YH, Yu TC. Muscarinic acetylcholine receptors present in human osteoblast and bone tissue. European journal of pharmacology. 2011;650(1):34-40.

54. Ternes S, Trinkaus K, Bergen I, et al. Impact of acetylcholine and nicotine on human osteoclastogenesis in vitro. International immunopharmacology. 2015;29(1):215-21.

55. Daley EJ, Pajevic PD, Roy S, Trackman PC. Impaired Gastric Hormone Regulation of Osteoblasts and Lysyl Oxidase Drives Bone Disease in Diabetes Mellitus. JBMR Plus. 2019;3(10):e10212.

56. Maffei A, Segal AM, Alvarez-Perez JC, Garcia-Ocana A, Harris PE. Anti-incretin, Anti-proliferative Action of Dopamine on beta-Cells. Mol Endocrinol. 2015;29(4):542-57.

57. Fothergill LJ, Furness JB. Diversity of enteroendocrine cells investigated at cellular and subcellular levels: the need for a new classification scheme. Histochem Cell Biol. 2018;150(6):693-702.

58. Cho HJ, Robinson ES, Rivera LR, et al. Glucagon-like peptide 1 and peptide YY are in separate storage organelles in enteroendocrine cells. Cell Tissue Res. 2014;357(1):63-9.

59. Eissele R, Goke R, Willemer S, et al. Glucagon-like peptide-1 cells in the gastrointestinal tract and pancreas of rat, pig and man. Eur J Clin Invest. 1992;22(4):283-91.

60. Holst JJ. The physiology of glucagon-like peptide 1. Physiol Rev. 2007;87(4):1409-39.

61. Cox HM. Peptide YY: a neuroendocrine neighbor of note. Peptides. 2007;28(2):345-51.

62. Holst JJ, Albrechtsen NJW, Gabe MBN, Rosenkilde MM. Oxyntomodulin: Actions and role in diabetes. Peptides. 2018;100:48-53.

63. Grunddal KV, Ratner CF, Svendsen B, et al. Neurotensin Is Coexpressed, Coreleased, and Acts Together With GLP-1 and PYY in Enteroendocrine Control of Metabolism. Endocrinology. 2016;157(1):176-94.

7. FIGURE LEGENDS

Figure 1: Bone phenotype in K-cell-deficient mice (GIP-DT mice). (A) Bone strength at the whole bone level was evaluated by destructive 3-point bending test. Maximum bending load and bending stiffness were not significantly different between animals. (B) Three dimensional microCT reconstruction of the proximal tibia metaphysis 800µm below the growth plate. (C) Bone microarchitecture estimated by microCT at the proximal tibia metaphysis in 16-week-old male mice. BV/TV: Trabecular bone volume, Ct.Th: Cortical thickness. (D) Number of osteoclasts (N.Oc/B.Pm) and bone formation rate (BFR/BS) were determined by histomorphometry at the proximal tibia metaphysis. (E) Bone strength at the bone matrix level estimated by nanoindentation. The nanoindentation force required to penetrate the diamond

Berkovich tip up to 900 nm (force) and indentation modulus (E_{IT}) are presented. (F) Mineral-to-matrix ratio (M/M ratio) and collagen maturity (XLR) were determined at bone formation site by Fourier transform infrared microspectroscopy. All results are presented as a boxplot (median, interquartile range). Statistical analyses have been performed with an unpaired two-tailed t-test. n = 7 mice in wild-type (WT) group, n = 8 mice in GIP-DT group.

Figure 2: Bone phenotype in GIP-deficient mice (GIP-KI mice). (A) Bone strength at the whole bone level was evaluated by destructive 3-point bending test. Maximum bending load and bending stiffness were not significantly different between animals although a trend was observed for stiffness (p=0.07). (B) Three dimensional microCT reconstruction of the proximal tibia metaphysis 800µm below the growth plate. (C) Bone microarchitecture estimated by microCT at the proximal tibia metaphysis in 16-week-old male mice. BV/TV: Trabecular bone volume, Ct.Th: Cortical thickness. (D) Number of osteoclasts (N.Oc/B.Pm) and bone formation rate (BFR/BS) were determined by histomorphometry at the proximal tibia metaphysis. (E) Bone strength at the bone matrix level estimated by nanoindentation. The nanoindentation force required to penetrate the diamond Berkovich tip up to 900 nm (force) and indentation modulus (E_{IT}) are presented. (F) Mineral-to-matrix ratio (M/M ratio) and collagen maturity (XLR) were determined at bone formation site by Fourier transform infrared microspectroscopy. All results are presented as a boxplot (median, interquartile range). Statistical analyses have been performed with an unpaired two-tailed t-test. n = 7 animals in each group.

Figure 3: Effects of administration of K-cell peptide analogues on bone remodeling, microarchitecture and bone composition in Swiss NIH mice. (A) The expression of K-cell product receptors in bone by quantitative PCR in whole bone extracts. (B) Whole bone strength was determined in 21 week old male swiss NIH mice administered daily with saline, 25

nmoles/kg [D-Ala²]GIP_{1-42} (GIP), 25 nmoles/kg xenin-25(Lys^{13}PAL) (xenin), 25 nmoles/kg (pGlu-Gln)cholecystokinin-8 (CCK-8), 25 nmoles/kg secretin or 30µg/kg RC160, a somatostatin receptor agonist for 6 weeks. (C) Three dimensional microCT reconstructions of the proximal tibia metaphysis 800µm below the growth plate. (D) Trabecular bone microarchitecture estimated by microCT at the proximal tibia metaphysis. BV/TV: Trabecular bone volume, Ct.Th: Cortical thickness. (E) Serum markers of bone remodeling. The N-terminal propeptide of type 1 collagen (P1NP), C-terminal type I collagen crosslinks (CTx-I), parathyroid hormone (PTH) and insulin-like growth factor-1 (IGF-1) levels were determined by ELISA. Ionized calcium was determined on an automated analyzer. (F) Osteoblast and osteoclast genes have been determined in whole bone extracts of saline-, [D-Ala²]GIP or xenin-25(Lys^{13}PAL)-treated mice. (G) Mineral-to-matrix ratio (M/M ratio), carbonate-to-phosphate ratio (C/P ratio) and collagen maturity (XLR) were determined at bone formation site by Fourier transform infrared microspectroscopy. (H) Expression of osteoblast genes involved in maturation of the bone matrix in whole bone extracts of saline-, [D-Ala²]GIP or xenin-25(Lys^{13}PAL)-treated mice. (I) Total GIP and total GLP-1 plasma levels were determined by ELISA in overnight fasted animals. All results are presented as a boxplot (median, interquartile range). Statistical analysis was performed by ANOVA, followed by Dunnett post-hoc test. n = 6 in saline, GIP, CCK-8, secretin or RC160 injected group, n = 5 in xenin injected group. a: p=0.021, b: p=0.024, c: p=0.006, d: p=0.003, e: p<0.0001 , f: p=0.056, g: p<0.0001 , h: p=0.0002, i: p<0.0001 , j: p=0.023, k: p<0.0001 , l: p=0.009, m: p<0.0001, n: p=0.064, o: p<0.0001 , p: p=0.074, q: p=0.004, r: p=0.005, s: p=0.006, t: p=0.004, u: p=0.003, v: p=0.003, w: p=0.0003, x: p=0.0001, y: p<0.0001, z: p=0.041, aa: p<0.0001, ab: p<0.0001, ac: p=0.002, ad: p=0.015, ae: p=0.0005, af: p=0.002 and ag: p=0.0002.

Figure 4: Effects of administration of xenin analogues or co-administration of GIP and xenin analogues on bone biomechanics, microarchitecture and bone composition (A and F) Bone strength was evaluated by destructive 3-point bending test. (B and G) Three dimensional microCT reconstruction of the proximal tibia metaphysis 800µm below the growth plate. (C and H) Bone microarchitecture estimated by microCT at the proximal tibia metaphysis. BV/TV: Trabecular bone volume, Ct.Th: Cortical thickness. (D) Number of osteoclasts (N.Oc/B.Pm) and bone formation rate (BFR/BS) were determined by histomorphometry at the proximal tibia metaphysis. (E and I) Mineral-to-matrix ratio (M/M ratio), carbonate-to-phosphate ratio (C/P ratio) and collagen maturity (XLR) were determined at bone formation site by Fourier transform infrared microspectroscopy. Bone parameters were evaluated in C57BL/6 (A-E) or Swiss (F-I) mice. All results are presented as a boxplot (median, interquartile range). Statistical analyses have been performed with an unpaired two-tailed t-test. n = 6 animals in each group.

Figure 5: GIP but not xenin directly affects bone cell physiology. (A) Human PBMCs were cultured in the presence of M-CSF, soluble human RANKL and saline, 1 nmole/L [D-Ala²]GIP or xenin-25(Lys^{13}PAL). Osteoclast numbers were counted per well at 18 days after TRAP staining. TRAP positive multinucleated cell (>3 nuclei) were counted as osteoclasts. In parallel, MC3T3-E1 cells were cultured with saline, 1 nmole/L [D-Ala²]GIP or xenin-25(Lys^{13}PAL) for 2 weeks and the extent of collagen maturity (XLR) was determined by Fourier transform infrared microspectroscopy. (B) Gene expression in osteoclast and osteoblast cultures after 7 days of treatment with saline, 1 nmole/L [D-Ala²]GIP or xenin-25(Lys^{13}PAL). Data represents 3-5 independent experiments performed each in triplicate. All results are presented as a boxplot (median, interquartile range). Statistical analysis was performed by ANOVA, followed by Dunnett post-hoc test.

Figure 6: Schematic representation of a plausible scenario of GIP and xenin in a physiological context. K-cell (Blue cell) are embedded in the proximal gut epithelium and expressed several gut hormones that possibly could be stored in separate secretion granules/vesicles. Among them GIP (blue granules) and Xenin (green granules) have been shown in the present study to exert different effects on bone. A plausible scenario would be represented by an early response from entry of nutrients in the gut lumen that would stimulate the secretion of GIP into the blood capillaries of the lamina propria. GIP would then stimulate bone anabolic pathways to build bone and store calcium into the bone mineral. A slower response could be then triggered by xenin secretion, by action on an unidentified target that in return could stop GIP anabolic action.

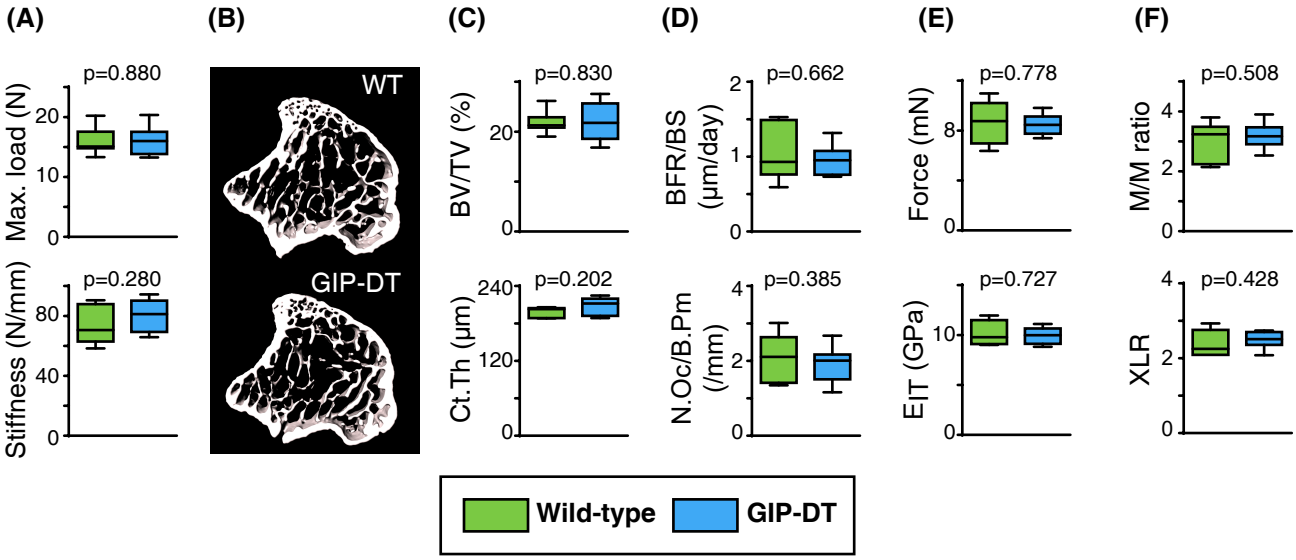
(A)
(B)
(C)
(D)
(E)
(F)
Max. load (N)
p=0.880
Stiffness (N/mm)
p=0.280
WT
GIP-DT
BV/TV (%)
p=0.830
Ct.Th (μm)
p=0.202
BFR/BS (μm/day)
p=0.662
N.Oc/B.Pm (/mm)
p=0.385
Force (mN)
p=0.778
EIT (GPa)
p=0.727
M/M ratio
p=0.508
XLR
p=0.428
Wild-type
GIP-DT

Figure 1

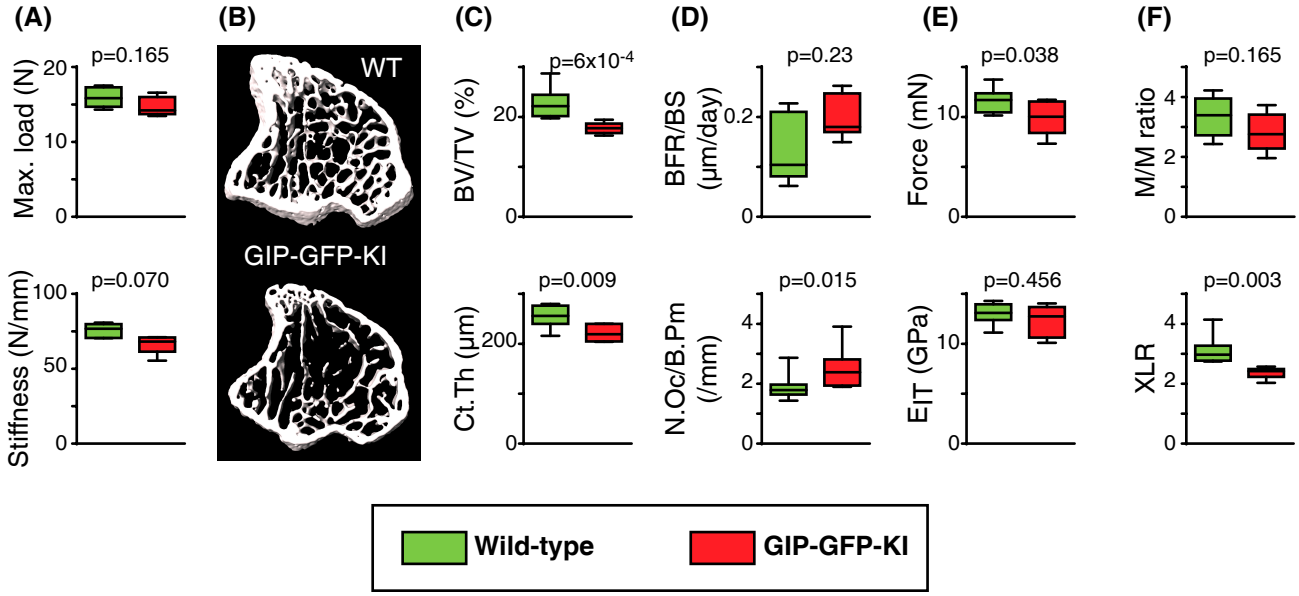
(A)
(B)
(C)
(D)
(E)
(F)
Max. load (N)
p=0.165
Stiffness (N/mm)
p=0.070
WT
GIP-GFP-KI
BV/TV (%)
p=6x10-4
Ct.Th (µm)
p=0.009
BFR/BS (µm/day)
p=0.23
N.Oc/B.Pm (/mm)
p=0.015
Force (mN)
p=0.038
EIT (GPa)
p=0.456
M/M ratio
p=0.165
XLR
p=0.003
Wild-type
GIP-GFP-KI

Figure 2

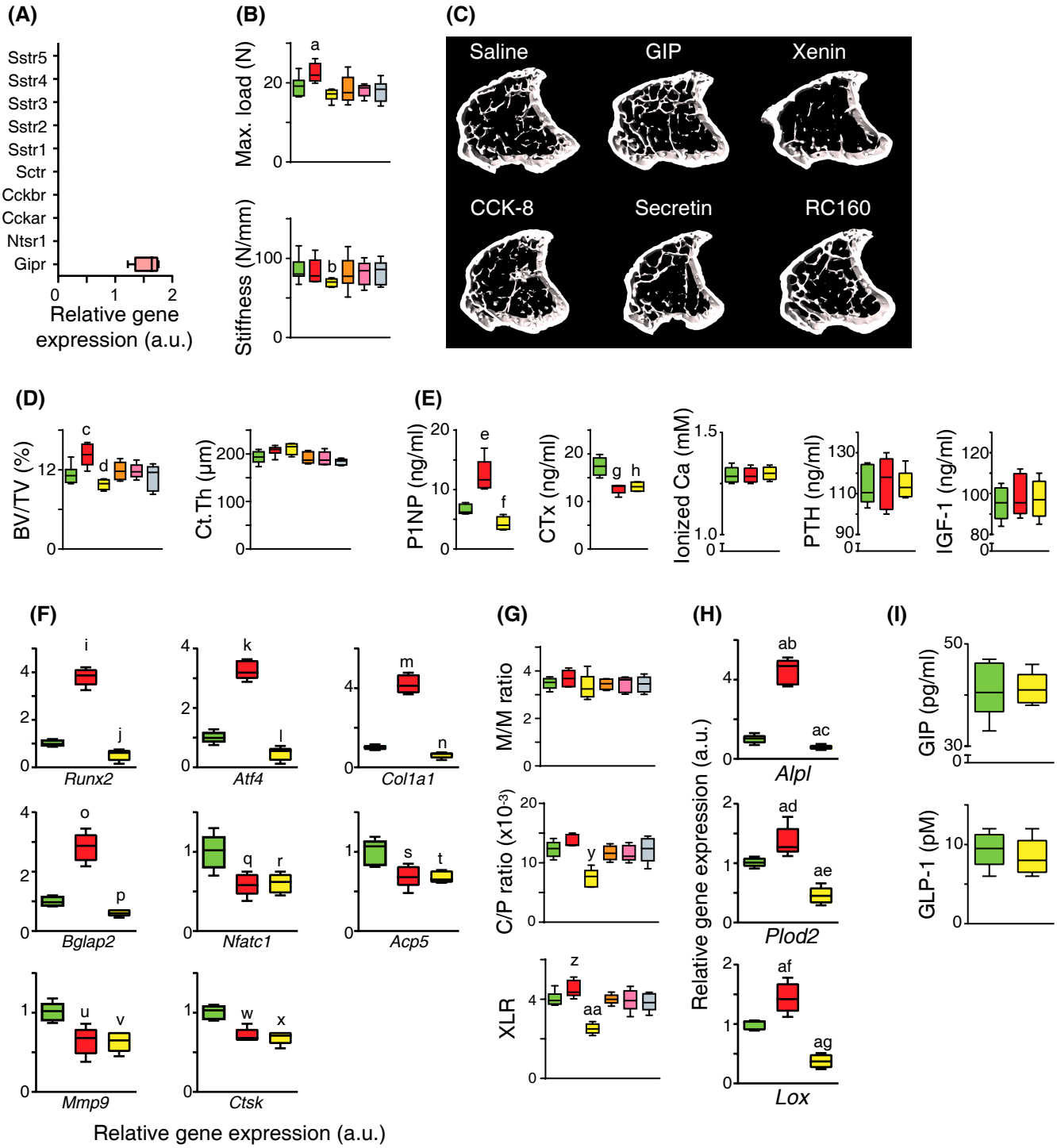
(A)
Sstr5
Sstr4
Sstr3
Sstr2
Sstr1
Sctr
Cckbr
Cckar
Ntsr1
Gipr
0
1
2
Relative gene expression (a.u.)
(B)
Max. load (N)
20
0
a
Stiffness (N/mm)
100
0
b
(C)
Saline
GIP
Xenin
CCK-8
Secretin
RC160
(D)
BV/TV (%)
12
0
c
d
Ct.Th (μm)
200
100
0
(E)
P1NP (ng/ml)
20
10
0
e
f
CTx (ng/ml)
20
10
0
g
h
Ionized Ca (mM)
1.5
1.0
0
PTH (ng/ml)
130
110
90
0
IGF-1 (ng/ml)
120
100
80
0
(F)
Runx2
i
j
Atf4
k
l
Col1a1
m
n
Bglap2
o
p
Nfatc1
q
r
Acp5
s
t
Mmp9
u
v
Ctsk
w
x
Relative gene expression (a.u.)
(G)
M/M ratio
C/P ratio (x10-3)
y
XLR
z
aa
(H)
Relative gene expression (a.u.)
Alpl
ab
ac
Plod2
ad
ae
Lox
af
ag
(I)
GIP (pg/ml)
50
30
0
GLP-1 (pM)
10
0
Saline
(pGlu-Gln)CCK-8
[D-Ala²]GIP1-42
Secretin
Xenin-25(Lys(13)PAL)
RC160

Figure 3

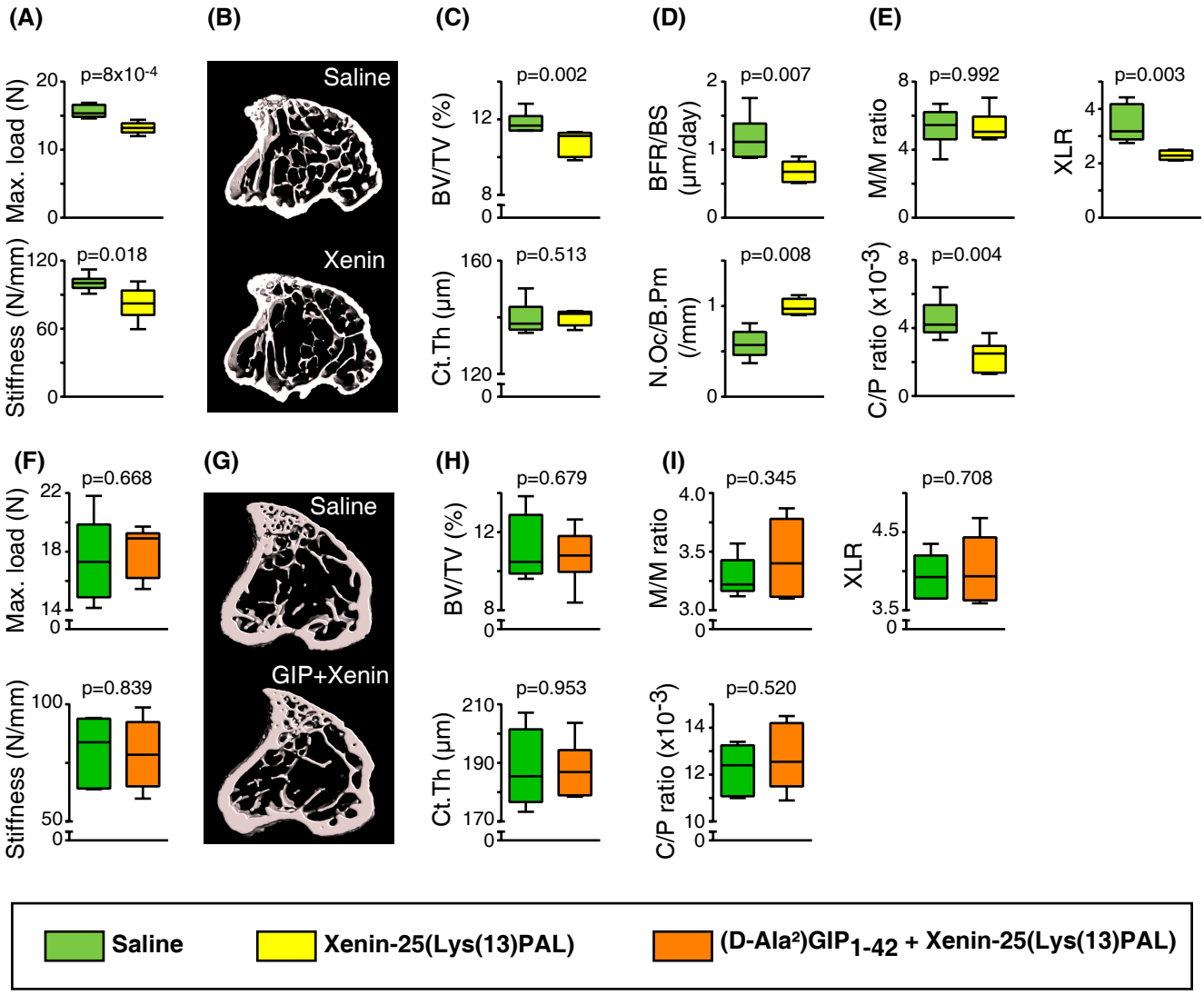
(A)
(B)
(C)
(D)
(E)
Max. load (N)
p=8x10-4
Stiffness (N/mm)
p=0.018
Saline
Xenin
BV/TV (%)
p=0.002
Ct.Th (µm)
p=0.513
BFR/BS (µm/day)
p=0.007
N.Oc/B.Pm (/mm)
p=0.008
M/M ratio
p=0.992
C/P ratio (x10-3)
p=0.004
XLR
p=0.003
(F)
(G)
(H)
(I)
Max. load (N)
p=0.668
Stiffness (N/mm)
p=0.839
Saline
GIP+Xenin
BV/TV (%)
p=0.679
Ct.Th (µm)
p=0.953
M/M ratio
p=0.345
C/P ratio (x10-3)
p=0.520
XLR
p=0.708
Saline
Xenin-25(Lys(13)PAL)
(D-Ala²)GIP1-42 + Xenin-25(Lys(13)PAL)

Figure 4

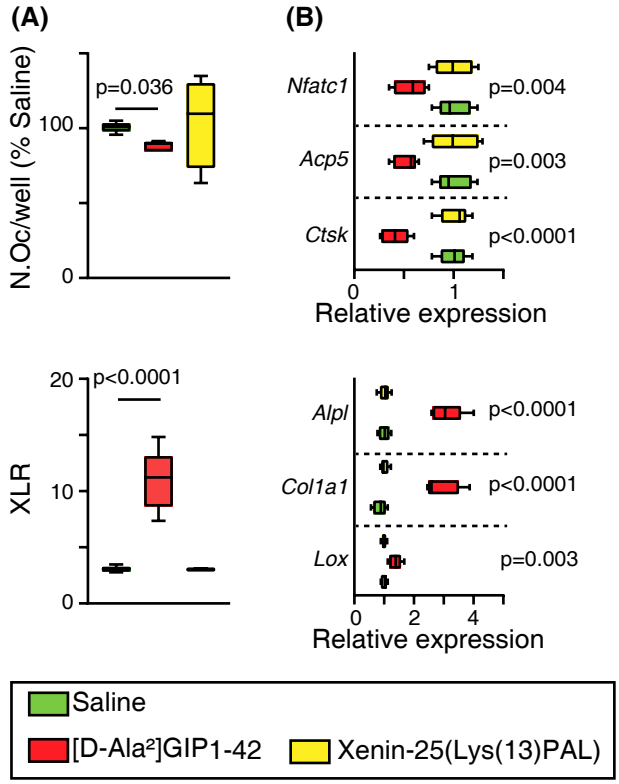
(A)
(B)
N.Oc/well (% Saline)
p=0.036
100
0
Nfatc1
p=0.004
Acp5
p=0.003
Ctsk
p<0.0001
0
1
Relative expression
XLR
20
p<0.0001
10
0
Alpl
p<0.0001
Col1a1
p<0.0001
Lox
p=0.003
0
2
4
Relative expression
Saline
[D-Ala²]GIP1-42
Xenin-25(Lys(13)PAL)

Figure 5

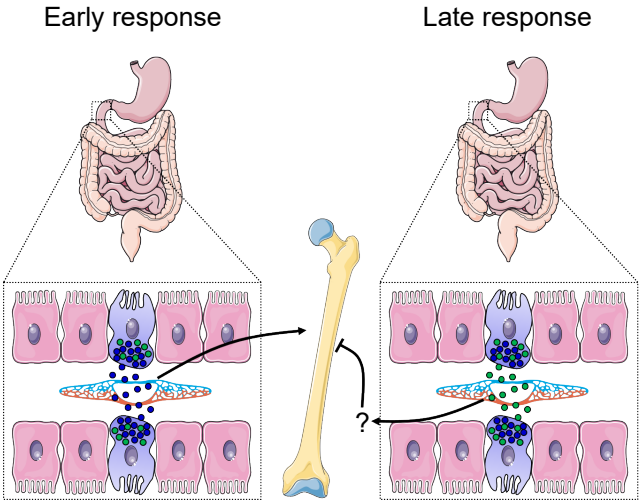

Figure 6

Supplementary table 1: Bone strength, trabecular microarchitecture, histomorphometry and compositional parameters in 16-week-old GIP-DT mice.

	Wild-type (n=7)	GIP-DT (n=8)	P values
Morphological parameters			
Body mass (g)	27.0 ± 0.6	27.0 ± 0.5	0.946
Femur length (mm)	13.6 ± 0.1	13.6 ± 0.1	0.920
Whole bone strength (3-point bending)			
Maximum bending load (N)	16.0 ± 0.9	16.1 ± 0.8	0.880
Maximum displacement (mm)	0.97 ± 0.10	0.95 ± 0.08	0.779
Bending stiffness (N/mm)	73.6 ± 4.8	80.4 ± 3.8	0.280
Work to fracture (N.mm)	8.4 ± 0.7	9.0 ± 0.5	0.445
Bone matrix strength (Nanoindentation)			
Indentation force (mN)	8.7 ± 0.7	8.5 ± 0.3	0.778
Indentation modulus (GPa)	10.2 ± 0.5	10.0 ± 0.3	0.727
Hardness (MPa)	474 ± 58	459 ± 19	0.999
Work of indentation (pJ)	2187 ± 144	2127 ± 67	0.999
Trabecular microarchitecture (MicroCT)			
BV/TV (%)	21.8 ± 0.8	22.2 ± 1.2	0.830
Tb.N (1/mm)	3.3 ± 0.2	3.4 ± 0.1	0.837
Tb.Th (µm)	66 ± 1	65 ± 2	0.874
Tb.Sp (µm)	185 ± 4	181 ± 3	0.299
Bone histomorphometry			
MAR (µm/day)	3.1 ± 0.3	3.3 ± 0.2	0.607
MS/BS (%)	32.6 ± 2.1	27.9 ± 1.5	0.142
BFR/BS (µm/day)	1.0 ± 0.2	0.9 ± 0.1	0.662
N.Oc/B.Pm (1/mm)	2.1 ± 0.2	1.9 ± 0.2	0.385
Oc.S/BS (%)	9.6 ± 1.1	8.1 ± 0.9	0.211
Bone mineral density distribution (qBEI)			
Ca_{mean} (%Ca)	21.0 ± 0.2	21.2 ± 0.2	0.470
Ca_{width} (% Ca)	3.1 ± 0.1	3.1 ± 0.1	0.918
Bone composition at bone formation site (Fourier transform infrared microspectroscopy)			
Mineral/matrix ratio	3.0 ± 0.3	3.2 ± 0.1	0.508
Carbonate/phosphate ratio	0.013 ± 0.002	0.013 ± 0.001	0.800
Mineral crystallinity	1.11 ± 0.04	1.05 ± 0.01	0.179
Acid phosphate content	0.49 ± 0.02	0.42 ± 0.02	0.071
Collagen maturity	2.4 ± 0.1	2.5 ± 0.1	0.428
Collagen glycation	0.004 ± 0.000	0.004 ± 0.000	0.722

Data are presented as mean ± SEM.

Supplementary table 2: Bone strength, trabecular microarchitecture, histomorphometry and compositional parameters in 16-week-old GIP-GFP-KI mice.

	Wild-type (n=7)	GIP-GFP-KI (n=7)	P values
Morphological parameters			
Body mass (g)	31.9 ± 0.4	32.1 ± 0.7	0.946
Femur length (mm)	13.8 ± 0.1	14.0 ± 0.1	0.328
Whole bone strength (3-point bending)			
Maximum bending load (N)	15.9 ± 0.5	14.9 ± 0.5	0.165
Maximum displacement (mm)	0.95 ± 0.08	1.17 ± 0.12	0.503
Bending stiffness (N/mm)	75.2 ± 1.7	68.0 ± 2.7	0.070
Work to fracture (N.mm)	9.5 ± 0.6	9.4 ± 0.7	0.922
Bone matrix strength (Nanoindentation)			
Indentation force (mN)	11.6 ± 0.5	9.7 ± 0.6	0.038
Indentation modulus (GPa)	12. ± 0.4	12.3 ± 0.6	0.456
Hardness (MPa)	636 ± 37	523 ± 32	0.053
Work of indentation (pJ)	3006 ± 160	2521 ± 188	0.128
Trabecular microarchitecture (MicroCT)			
BV/TV (%)	22.7 ± 1.1	17.7 ± 0.4	<0.001
Tb.N (1/mm)	3.4 ± 0.1	2.7 ± 0.1	<0.001
Tb.Th (µm)	67 ± 1	65 ± 1	0.375
Tb.Sp (µm)	187 ± 3	202 ± 4	0.014
Bone histomorphometry			
MAR (µm/day)	1.1 ± 0.1	1.2 ± 0.1	0.275
MS/BS (%)	13.1 ± 1.9	15.4 ± 1.8	0.495
BFR/BS (µm/day)	0.13 ± 0.02	0.20 ± 0.02	0.023
N.Oc/B.Pm (1/mm)	1.9 ± 0.2	2.5 ± 0.2	0.015
Oc.S/BS (%)	8.5 ± 0.7	12.1 ± 1.0	0.015
Bone mineral density distribution (qBEI)			
Ca_{mean} (% Ca)	21.0 ± 0.7	22.1 ± 0.7	0.275
Ca_{width} (%Ca)	3.4 ± 0.1	3.5 ± 0.1	0.290
Bone composition at bone formation site (Fourier transform infrared microspectroscopy)			
Mineral/matrix ratio	3.4 ± 0.2	2.8 ± 0.2	0.165
Carbonate/phosphate ratio	0.008 ± 0.001	0.007 ± 0.001	0.603
Mineral crystallinity	1.06 ± 0.04	1.02 ± 0.05	0.558
Acid phosphate content	0.70 ± 0.05	0.78 ± 0.08	0.603
Collagen maturity	3.1 ± 0.2	2.4 ± 0.1	0.003
Collagen glycation	0.004 ± 0.001	0.004 ± 0.000	0.832

Data are presented as mean ± SEM.

Supplementary table 3: Bone strength, trabecular microarchitecture, histomorphometry and compositional parameters after 6 weeks treatment with saline, [D-Ala^2]GIP$_{1-42}$, Xenin-25(Lys(13)PAL), (pGlu-Gln)CCK-8, secretin or RC160 in NIH Swiss mice.

	Saline	GIP	Xenin	CCK-8	Secretin	RC160
Morphological parameters						
Body mass (g)	26.9 ± 1.1	26.0 ± 1.4	25.1 ± 1.7	25.0 ± 1.0	25.8 ± 1.3	26.2 ± 1.6
Femur length (mm)	16.3 ± 0.1	16.4 ± 0.1	16.3 ± 0.1	16.3 ± 0.1	16.3 ± 0.1	16.3 ± 0.1
Whole bone strength (3-point bending)						
Maximum bending load (N)	19.1 ± 0.9	**22.5 ± 1.0**	17.0 ± 0.6	18.3 ± 1.3	18.1 ± 0.5	17.9 ± 0.9
Maximum displacement (mm)	0.6 ± 0.1	0.8 ± 0.1	0.6 ± 0.1	0.6 ± 0.1	0.7 ± 0.1	0.6 ± 0.1
Bending stiffness (N/mm)	86 ± 6	84 ± 7	**70 ± 2**	82 ± 8	82 ± 5	83 ± 5
Work to fracture (N.mm)	7.0 ± 1.1	8.5 ± 1.2	6.8 ± 1.1	6.7 ± 0.8	7.0 ± 0.8	6.1 ± 0.8
Trabecular microarchitecture (MicroCT)						
BV/TV (%)	18.8 ± 1.0	**23.7 ± 1.2**	**16.3 ± 0.6**	19.7 ± 1.0	19.7 ± 0.7	18.2 ± 1.3
Tb.N (1/mm)	3.0 ± 0.1	**3.5 ± 0.1**	**2.4 ± 0.1**	2.9 ± 0.1	2.9 ± 0.1	2.8 ± 0.2
Tb.Th (µm)	65 ± 1	65 ± 1	66 ± 2	67 ± 1	66 ± 1	64 ± 1
Tb.Sp (µm)	240 ± 9	**189 ± 6**	**276 ± 13**	234 ± 8	240 ± 8	250 ± 12
Bone histomorphometry						
MAR (µm/day)	2.9 ± 0.3	3.5 ± 0.2	2.7 ± 0.2	3.0 ± 0.2	3.0 ± 0.3	2.7 ± 0.3
MS/BS (%)	51.7 ± 1.6	**61.2 ± 2.1**	**43.5 ± 1.4**	52.8 ± 1.6	49.9v 1.6	49.4 ± 2.4
BFR/BS (µm/day)	1.5 ± 0.2	**2.1 ± 0.1**	*1.1 ± 0.1*	1.6 ± 0.1	1.5 ± 0.2	1.3 ± 0.1
N.Oc/B.Pm (1/mm)	0.75 ± 0.15	**0.25 ± 0.04**	*0.49 ± 0.09*	0.78 ± 0.14	0.82 ± 0.16	0.81 ± 0.16
Bone matrix strength (Nanoindentation)						
Indentation force (mN)	12.2 ± 0.4	13.2 ± 0.5	**14.3 ± 0.3**	12.3 ± 0.4	12.3 ± 0.4	12.0 ± 0.5
Indentation modulus (GPa)	14.0 ± 0.4	15.3 ± 0.5	**16.1 ± 0.4**	13.9 ± 0.5	14.4 ± 0.6	14.8 ± 0.5
Hardness (MPa)	717 ± 10	735 ± 8	**877 ± 43**	705 ± 9	703 ± 9	697 ± 8
Work of indentation (pJ)	2724 ± 159	3078 ± 249	2902 ± 71	2796 ± 289	2748 ± 307	2524 ± 161
Bone composition at bone formation site (Fourier transform infrared microspectroscopy)						
Mineral/matrix ratio	3.5 ± 0.1	3.7 ± 0.1	3.3 ± 0.2	3.4 ± 0.1	3.5 ± 0.1	3.4 ± 0.1
Carb./phosphate ratio (x10^3)	12.3 ± 0.6	13.7 ± 0.4	**7.4 ± 0.6**	11.7 ± 0.5	11.6 ± 0.6	12.2 ± 0.9
Mineral crystallinity	1.02 ± 0.01	1.02 ± 0.01	1.16 ± 0.10	1.02 ± 0.02	1.01 ± 0.02	1.01 ± 0.01
Acid phosphate content	0.73 ± 0.04	0.66 ± 0.04	0.83 ± 0.13	0.72 ± 0.08	0.70 ± 0.06	0.68 ± 0.09
Collagen maturity	4.0 ± 0.1	**4.5 ± 0.2**	**2.5 ± 0.1**	4.0 ± 0.1	3.9 ± 0.2	3.8 ± 0.2

Data are presented as mean ± SEM. Significant modifications as compared with saline-treated animals ($p<0.05$) are highlighted in bold, and statistical trends (p values between 0.05 and 0.1) are in italic.n=6 mice/group except for xenin-25(Lys(13)PAL)-treated animals where 5 mice/group were used.